The EMBO Journal (2007) 26, 3484–3493 | © 2007 European Molecular Biology Organization | Some Rights Reserved 0261-4189/07
www.embojournal.org

THE EMBO JOURNAL

EMBO open

Structure of the APPL1 BAR-PH domain and characterization of its interaction with Rab5

Guangyu Zhu[1], Jia Chen[2], Jay Liu[3], Joseph S Brunzelle[4], Bo Huang[2], Nancy Wakeham[1], Simon Terzyan[1], Xuemei Li[2], Zihe Rao[2], Guangpu Li[3] and Xuejun C Zhang[1,2,*]

[1]Crystallography Research Program, Oklahoma Medical Research Foundation, Oklahoma City, OK, USA, [2]National Laboratory of Biomacromolecules, Institute of Biophysics, Chinese Academy of Sciences, Beijing, China, [3]Department of Biochemistry and Molecular Biology, University of Oklahoma Health Sciences Center, Oklahoma City, OK, USA and [4]Department of Molecular Pharmacology and Biological Chemistry, Feinberg Medical School, Northwestern University, Chicago, IL, USA

APPL1 is an effector of the small GTPase Rab5. Together, they mediate a signal transduction pathway initiated by ligand binding to cell surface receptors. Interaction with Rab5 is confined to the amino (N)-terminal region of APPL1. We report the crystal structures of human APPL1 N-terminal BAR-PH domain motif. The BAR and PH domains, together with a novel linker helix, form an integrated, crescent-shaped, symmetrical dimer. This BAR–PH interaction is likely conserved in the class of BAR-PH containing proteins. Biochemical analyses indicate two independent Rab-binding sites located at the opposite ends of the dimer, where the PH domain directly interacts with Rab5 and Rab21. Besides structurally supporting the PH domain, the BAR domain also contributes to Rab binding through a small surface region in the vicinity of the PH domain. In stark contrast to the helix-dominated, Rab-binding domains previously reported, APPL1 PH domain employs β-strands to interact with Rab5. On the Rab5 side, both switch regions are involved in the interaction. Thus we identified a new binding mode between PH domains and small GTPases.

The EMBO Journal (2007) **26,** 3484–3493. doi:10.1038/sj.emboj.7601771; Published online 21 June 2007
Subject Categories: proteins; structural biology
Keywords: APPL1; BAR-PH domain; Rab5; signaling endosome; trafficking

*Corresponding author. Crystallography Research Program, Oklahoma Medical Research Foundation, 825 NE 13th Street, Oklahoma City, OK 73104, USA. Tel.: +1 405 271 7402; Fax: +1 405 271 7953; E-mail: zhangc@omrf.ouhsc.edu

Received: 21 March 2007; accepted: 30 May 2007; published online: 21 June 2007

Introduction

Endocytosis induced by ligand–receptor interaction has been directly linked to signal transduction mediated by Rab5 and its effector APPL1 (*A*daptor protein containing *P*H domain *P*TB domain and *L*eucine zipper motif; Miaczynska *et al*, 2004; Mao *et al*, 2006). The small GTPase Rab5 is a generally acknowledged prominent regulator of vesicle trafficking enroute from the plasma membrane to early endosomes (Li, 1996), whereas APPL1 (also called DIP13α) is identified with signaling pathways of adiponectin, insulin, EGF, follicle stimulating hormone receptor, neurotrophin receptor (TrkA), oxidative stress, and DCC-mediated apoptosis (Liu *et al*, 2002; Miaczynska *et al*, 2004; Lin *et al*, 2006; Mao *et al*, 2006; Varsano *et al*, 2006; Nechamen *et al*, 2007). Within this milieu, APPL1 specifically binds to the GTP-bound, active form of Rab5. In response to extracellular stimuli, Rab5 hydrolyzes its bound GTP, releasing APPL1 from an endocytic structure, and allowing APPL1 to further interact with components of nucleosome remodeling and histone deacetylase complexes. The interaction with Rab5 is essential for APPL1 localization to the endosomes and is indispensable for the functional cycle of APPL1 (Miaczynska *et al*, 2004).

Human APPL1, a multidomain protein 709 amino-acid (aa) residues in length contains an amino (N)-terminal BAR (*B*in1/*A*mphiphysin/*R*VS167) domain and a PH (*p*leckstrin *h*omology) domain followed by a carboxy (C)-terminal PTB (*p*hospho*t*yrosine *b*inding) domain (Sakamuro *et al*, 1996; Liu *et al*, 2002; Miaczynska *et al*, 2004). The Rab5-binding site is located in the N-terminal BAR-PH region (Miaczynska *et al*, 2004), while the C-terminal region is found to interact with a host of other proteins, including the adiponectin receptor (Mao *et al*, 2006), Akt2/PKBβ kinase (Mitsuuchi *et al*, 1999), tumor suppressor DCC (Liu *et al*, 2002), TrkA, and TrkA interacting protein GIPC1 (Lin *et al*, 2006).

Based on aa sequence analysis, BAR domains have been identified in many proteins involved in intracellular trafficking, but sequence homology is low in general among known BAR domains (Farsad *et al*, 2001; Habermann, 2004). The BAR domain typically contains three long kinked α-helices (α1, α2, and α3) that form a well-packed, crescent-shaped, symmetrical, six-helix bundle, side-by-side antiparallel homodimer; a structure proposed to exert its function as a convex membrane-curvature sensor or stabilizer. The concave surface of the BAR dimer is proposed to bind preferentially to a negatively charged, curved membrane largely through electrostatic interactions. Furthermore, some BAR domains have been found to bind to small GTPases, a class of intracellular molecular switches (Tarricone *et al*, 2001; Habermann, 2004); thus, their membrane association is directly linked to regulation of signal transduction and trafficking. However, currently available structural information

suggests that bindings of the BAR domain to GTPases and to membrane lipids are incompatible, because both interactions appear to compete for the same concave surface region of the BAR dimer (Tarricone *et al*, 2001). The BAR domain of APPL1 is required for Rab5 binding and membrane recruitment (Miaczynska *et al*, 2004), although the mechanisms remain to be elucidated.

The PH domain is approximately 100-residue long, and has been identified in over 100 different eukaryotic proteins such as kinases, isoforms of phospholipase C (PLC), GTPases, and their regulators; most of which participate in cell signaling and cytoskeletal regulation (Rebecchi and Scarlata, 1998). Despite their minimal sequence homology, the three-dimensional (3D) structures of PH domains are remarkably conserved. They possess a common core consisting of seven β-strands and a C-terminal α-helix (Rebecchi and Scarlata, 1998). Some PH domains specifically bind to phosphatidylinositol phosphates, suggesting that one possible function of this family is to anchor the host proteins to membranes. PH domains are also suggested to bind to the Gβγ complex of the heterotrimeric G protein, protein kinase C, and small GTPases. Nevertheless, none of these functions is absolutely conserved. For instance, the PH domain of APPL1 alone is insufficient for binding to the membrane (Miaczynska *et al*, 2004). The PH domain immediately follows the C-terminus of the BAR domain; such a BAR-PH motif is essential for Rab5 binding. The same motif has also been found in a homolog Rab5 effector APPL2, centaurin-β family members, GRAF2, and oligophrenin (Habermann, 2004), but the 3D structure organization of BAR-PH motif and its functional implication remained elusive until now.

In order to address the functional roles of the BAR-PH motif in APPL1 and related proteins, we have carried out structure-function studies on human APPL1 and determined the crystal structures of the Rab5-binding region of APPL1 as well as the BAR domain alone. The results show that two BAR-PH molecules form an integrated, symmetric homodimer, and the PH domain has extensive intermolecular interactions with the BAR domain. The BAR dimer of APPL1 has a stronger curvature than other reported BAR structures. Further mutagenesis analyses allowed us to identify the binding sites on both APPL1 and Rab5. In sharp contrast to the presumed conflict between concurrent membrane association and GTPase binding by the BAR dimer (Habermann, 2004), the novel binding mode of the BAR-PH dimer should permit simultaneous interactions with both.

Results

Protein expression and crystallography

Recombinant proteins of human APPL1 N-terminal fragments including the BAR (residues 5–265) and BAR-PH domains (residues 5–385) were expressed in *Escherichia coli*, then purified using His tag affinity chromatography. The samples were crystallized after removing the tag with thrombin, which generated a four-residue (Gly–Ser–His–Met) peptide N-terminal to the native Asp5 residue.

The BAR domain crystal diffracted up to 1.8-Å resolution on a beamline at the Argonne Advanced Photon Source (APS) synchrotron facility. The crystal belongs to $P2_12_12$ space group. Phases of the structural factors were determined using the Se-Met-based single-wavelength anomalous dispersion (SAD) method (Supplementary data). There is one APPL1 BAR molecule per asymmetric unit, with ~41% solvent content. Regions of the N-terminus (up to Thr12), Leu75–Asp79, and C-terminus (i.e., Pro260–Asp265) were missing from the final refined model because of lack of interpretable electron density.

The BAR-PH crystal diffracted to 2.05-Å resolution at the synchrotron facility. The crystal also belongs to $P2_12_12$ space group. There is one APPL1 BAR-PH molecule per asymmetric unit, with ~45% solvent content. Phases of this crystal form were calculated using a combination of molecular replacement and SAD methods, and further improved with density modification. Regions of N-terminal non-native tripeptide (i.e., Gly–Ser–His), Gly76–Asp78, Asn288–Ser295, and C-terminus (i.e., Ser380–Glu385) lacked interpretable electron density and were omitted from the final refined model. Data collection and refinement statistics are summarized in Table I.

Table I Crystallography data collection and refinement statistics

(a) Data statistics	BAR	BAR–PH
Wavelength (Å)	0.9793	1.0000
Space group	$P2_12_12$	$P2_12_12$
Unit cell		
a (Å)	53.0	103.7
b	129.2	105.7
c	36.9	36.4
Resolution (Å)	50 (1.86)[a]–1.80	50 (2.12)–2.05
R_{merge} (%)	8.1 (44.0)	6.7 (43.2)
Number of reflections	23 548 (1897)	23 286 (1989)
Completeness (%)	96.1 (78.5)	89.9 (78.0)
Redundancy	3.3 (3.1)	4.5 (3.2)
$I/\sigma(I)$	10.2 (2.2)	16.4 (2.7)
(b) Refinement statistics		
$R_{working}$ (%)/# of reflections[b]	21.2/21 703	20.5/20 882
R_{free} (%)/# of reflections[b]	25.5/1200	26.8/1200
Number of non-hydrogen atoms		
Protein	1990	2943
Solvent	147	157
R.m.s.d. from ideal values		
Bond length (Å)/angle (deg)	0.016/1.51	0.013/1.30
Ramachandran plot (%)[c]	98.3/1.7/0/0	94.7/5.3/0/0
Average B-factor (Å^2)		
Protein	34.1 (25.8)[d]	47.9 (38.3)[d]
Solvent	41.4	47.7

[a]Numbers in parentheses are the corresponding numbers for the highest-resolution shell, unless otherwise mentioned.
[b]Reflections of $|F_{obs}| > 0.0$.
[c]Calculated using PROCHECK. Numbers reflect the percentage of residues in the core, allowed, generously allowed and disallowed regions, respectively.
[d]Wilson B-factors calculated using a 4 Å cutoff.

BAR domain structure and dimerization

From the two crystal forms of APPL1 peptides, we obtained two crystallographically independent BAR domain models. In both cases, the APPL1 BAR domain has three long helices, namely α1, α2, and α3. In addition, the APPL1 BAR domain contains an extra nine-turn α-helix, α4 (Figure 1; Supplementary Figure 1). The two models could be superimposed onto each other with a moderate, 1.3-Å, Cα-atom root mean square deviation (r.m.s.d.) if flexible terminal and loop regions (i.e., residues 5–18, 75–79, 151–153, and 255–265) were omitted. Thus, the overall structure of the BAR domain remains the same either alone or in the context of BAR-PH motif.

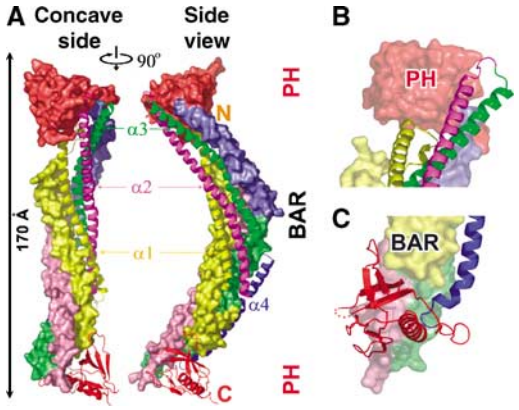

Figure 1 Crystal structure of the APPL1 BAR-PH dimer. (**A**) The overall structure of the dimer. The left view is along the direction of the dyad symmetry and on the concave surface, and the right view differs by 90°. One protomer is shown in ribbon diagram, and the other is shown in molecular surface model. Helix α1 is colored yellow, α2 magenta, α3 green, α4 blue, and PH domain red. (**B, C**) A close view of the BAR–PH interface. These images were generated using the program PyMol.

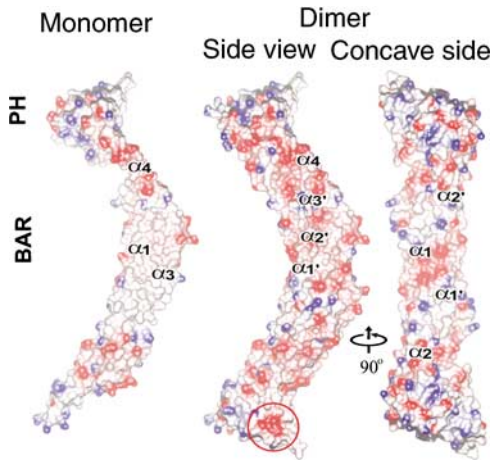

Figure 2 Electrostatic potential distribution of APPL1. Electrostatic potentials of APPL1 BAR-PH protomer (left) and dimer (middle and right) are mapped on their molecular surfaces. Negatively charged regions ($\leqslant -0.5$ V) are colored red, positively charged regions ($\geqslant +0.5$ V) blue, and neutral regions gray. The right view is looking down along the dyad axis of the dimer at the concave surface, and the side view differs by 90°. Clusters of acidic residues which are potentially important in Rab5 binding are circled. This figure was generated with the program CCP4mg.

In each of the two crystal forms, two BAR molecules form a tightly packed dimer, which assumes a crescent-like shape, a hallmark of the BAR dimer structure (Figure 1). In the BAR dimer, the helix α1 forms an antiparallel helix bundle with its symmetry counterpart, giving shape to the concave surface of the crescent-like dimer. Helix α4 packs against α3 of the symmetry mate on the convex side of the dimer, and its C-terminus points to the tip of the crescent. Over 4400 Å^2 solvent accessible surface (SAS) from each protomer is buried in the dimer interface. The addition of each α4 helix to the canonical BAR motif results in approximate 1900 Å^2 buried SAS on the two protomers, corresponding to over 40% of the total buried SAS.

Although the overall folding of APPL1 BAR domain is similar to previously reported BAR domain 3D structures (i.e., arfaptin2, PDB file 1I4T; amphiphysin, 1URU; and endophilin, 1ZWW), those structures are in general more similar to each other than to the APPL1 BAR domain. For instance, using 150 Cα atoms of the common helical regions, the r.m.s.d. values between the dimer of APPL1 BAR and 1I4T, 1URU, and 1ZWW were 3.7, 3.8, and 4.4 Å, respectively, while those among 1I4T, 1URU, and 1ZWW range between 2.4 and 2.6 Å. In addition, the APPL1 α1 and α2 helices lack extensive patches of positively charged aa residues on the concave surface (Figure 2); such patches are thought to be essential for some BAR containing proteins to induce *in vitro* tubule formation (Carlton *et al*, 2004).

The curvature of the concave face of the BAR dimer is thought to play an important role in membrane bending and/or curvature sensing (Habermann, 2004). We implemented a computing algorithm to calculate the curvature radius (r_C) and found that the APPL1 BAR dimer has an r_C about 55 Å (Supplementary data; Supplementary Figure 2), significantly smaller than the r_C values of other BAR dimers (Peter *et al*, 2004). Thus, the APPL1 BAR dimer has the strongest curvature among known BAR dimer structures.

Structure of the APPL1 PH domain

The APPL1 PH domain encompasses residues Asn276–Leu379 and has a typical PH folding (Supplementary Figure 3). The core structure of PH domain consists of a pair of nearly orthogonal β-sheets of four and three antiparallel β-strands (β1–β2–β3–β4 and β5–β6–β7; Supplementary Figure 1). The C-terminal α-helix, α_C, packs against both β-sheets and contributes to the core of the domain. In the PH domain, connecting loops are named after the preceding β-strands (e.g., the loop between β1 and β2 is called L1, etc). The canonical ligand-binding site is composed of β1, L1, β2, L3, and L6 (exemplified in the crystal structure of PLC-δ1, PDB file 1MAI) and, roughly speaking, is confined to a triangular area with L1, L3, and L6 as the three vertices. Some positively charged or polar residues that have been previously identified as critical for lipid binding in this ligand-binding triangle are not conserved in APPL1 (Supplementary Figures 1 and 3), consistent with the fact that APPL1 alone lacks membrane binding ability.

Packing of the BAR and PH domains

In our crystal structure of the APPL1 BAR-PH dimer, the two PH domains are located at the opposite ends of the crescent-shaped dimer, and each has fairly extensive contact with the BAR domain of its symmetry mate (Figure 1). The addition of the PH domain expands the BAR dimer in the longest dimension from 140 to 170 Å, but hardly changes the height of the dimer (i.e., the dimension along the two-fold axis direction) and its curvature. Using its β1, β2, L3, and L7 regions, the PH domain contacts the BAR domain of its symmetry mate in two places (Figures 1B, C and 3; Supplementary Figure 3). First, the motif of D^{15}SPxxR^{20} (where x stands for any aa residue) at the N-terminal of BAR domain contacts β1, β2, and L3 regions of PH domain. For instance, the hydroxyl group of Tyr283 in β1 forms a 2.6-Å hydrogen bond with the backbone carbonyl oxygen of Asp15 (Figure 3A). Second, the conserved D^{334}xxDRRYCF^{342} motif in the loop L7 of the PH domain is directly in contact with the loop connecting α2 and α3 in the BAR domain (Figure 3B). The buried SAS from each BAR-PH molecule in

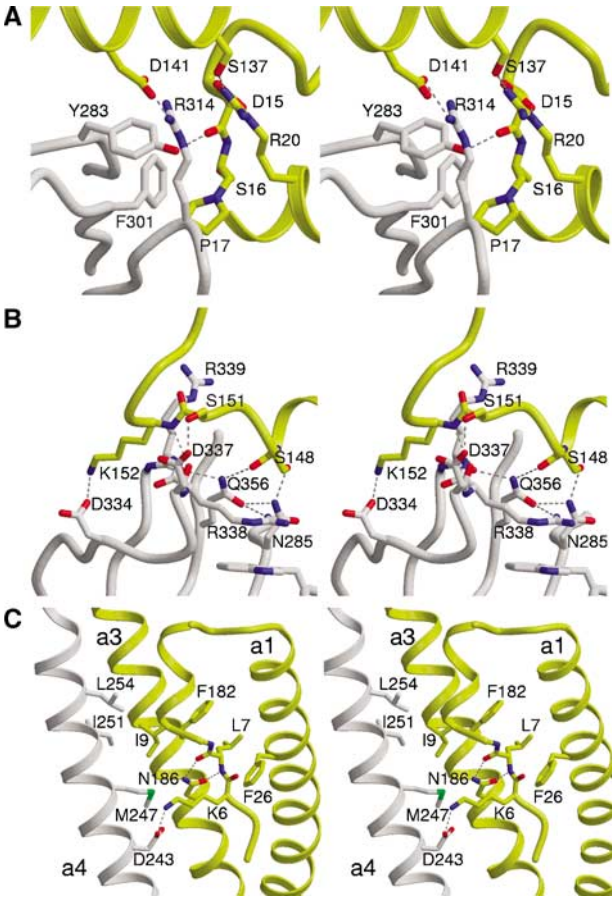

Figure 3 APPL1 domain packing. (**A, B**), Stereoviews of two major interacting regions between the PH and BAR domains. The PH domain from one APPL1 protomer is colored gray, and the BAR domain from the dimer-mate is colored yellow. Helix backbones are shown in ribbon representation, otherwise in ropes. Side-chain and/or main-chain atoms of selected residues are shown in stick models. Nitrogen atoms are colored blue, oxygen red, and sulfur green. Hydrogen bonds (<3.0 Å) are shown as dash-lines. Note that most residues displayed are highly conserved among the known BAR-PH containing proteins (Supplementary Figure 1). (**C**) Stereoview of interactions of the APPL1 N-terminal region. The two protomers are colored gray and yellow, respectively. This figure was generated with the programs Molscript and Raster3D.

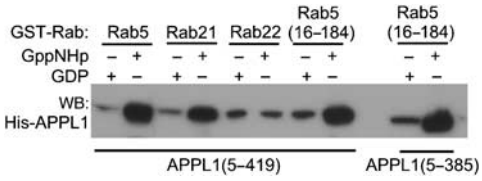

Figure 4 Pull-down analysis of APPL1-Rab interaction. GST fusion proteins of Rab5, Rab21, and Rab22 were used to pull down His-tagged APPL1 (5–385) and (5–419) fragments in the presence of GDP or GTP analog (GppNHp). The results were analyzed with SDS–PAGE and anti-His Western blot.

the dimer is about 6600 Å^2. Thus, in the presence of PH domain, the buried SAS is 50% larger than that of the dimer formed by BAR domain alone (4400 Å^2). The canonical 'ligand'-binding triangle of the PH domain is oriented about 60° from the concave side of the BAR dimmer, so that both the PH triangle and BAR concave surface could be brought within the vicinity of a curved membrane simultaneously. Nevertheless, as discussed earlier, key residues for lipid interaction are not conserved in APPL1. The C-terminus of PH is exposed to solvent in the dimer, consistent with the fact that it connects to the C-terminal region including the PTB domain.

Because of the interaction between D^{15}SPxxR^{20} motif and PH domain, the rest N-terminus peptide (residues 5–12) clearly became ordered in the BAR-PH crystal structure, in comparison to the BAR domain-alone crystal structure, where residues N-terminal to Leu13 were invisible in the electron density map. The fixed N-terminal peptide in the BAR-PH structure has an extended backbone conformation between Met4 (remnant from the His-tag cleavage) and Pro8, followed by a one-turn 3_{10} helix (Figure 3C). This region has several important intramolecular contacts mainly with helices α1 and α3. For instance, the Leu7 side chain inserts between the aromatic rings of Phe26 in α1 and Phe182 in α3. Meanwhile, the side chain of Asn186 forms two hydrogen bonds with the backbone amide and carbonyl groups of Leu7, respectively. All these hydrophobic and hydrogen bond interactions appear conserved among BAR-PH containing proteins (Supplementary Figure 1). Furthermore, the N-terminus is surrounded by a number of regions from the dimer partner, including the helix α4 and flexible loop connecting α1 and α2 (where residues 76–78 were mobile in the crystal structure). For instance, Lys6' (where the prime stands for the dimer partner) forms a salt bridge with Asp243 in α4 between the protomers. In addition, Ile9' forms hydrophobic interactions with Met247, Ile251, and Leu254 in α4 (Figure 3C).

To investigate roles of the BAR–PH interaction in solution, a double point mutation, S16E/P17E, at the BAR–PH interface was made. These residues are located in the region N-terminal to the BAR domain and form close contacts with β2 and L3 of the PH domain (Figure 3A). The recombinant protein of S16E/P17E double mutant in the context of BAR-PH was expressed predominantly in the insoluble fraction of cell lysate; however, the same mutations behaved normal in the BAR-only construct (data not shown). Moreover, expression of the APPL1 PH domain alone in *E. coli* did not produce soluble recombinant protein. The data suggest that the dimer interaction between PH and BAR domains is critical for the solubility and stability of the APPL1 PH domain. Consistent with this, our analytical ultracentrifugation (AUC) data showed that BAR-PH protein has a higher dimerization affinity in solution (k_d = 0.34 nM) than BAR domain alone (k_d = 0.13 μM; Supplementary data).

APPL1–Rab5 interaction in solution

To study APPL1–Rab5 interaction in solution, we performed glutathione *S*-transferase (GST)-mediated pull-down assays. The APPL1 BAR-PH domain (residues 5–385) and a longer fragment with a 40-residue extension downstream of the PH domain, APPL1 (5–419), were each effectively pulled down by GTP-bound GST–Rab5 fusion protein (Figure 4). The APPL1 protein was pulled down by either WT Rab5 preloaded with non-hydrolysable GTP analog (GppNHp) or Rab5-Q79L defective in GTP hydrolysis (with or without preloaded GTP analog), but could not be effectively pulled down by either the WT Rab5 preloaded with GDP or Rab5-S34N defective in GTP binding (Figure 4 and data not shown). In contrast to the BAR-PH domain, we confirmed

that APPL1 BAR domain alone (residues 5–265) cannot directly interact with Rab5 (data not shown) (Miaczynska *et al*, 2004). Furthermore, using different Rab5 truncation variants, we demonstrated that the N-terminus (residues 1–15) and C-terminus (residues 185–215) of Rab5 are dispensable for interaction with APPL1 (Figure 4).

Binding affinity between full-length Rab5-Q79L and APPL1 (5–419) was quantitatively determined in a surface plasmon resonance (SPR) experiment. Rab5 was coupled to the SPR biosensor chip in random orientations, and APPL1 (5–419) was applied as the analyte at concentrations of 0.15–12 μM (Supplementary Figure 4). The dissociation constant, k_d, for the Rab5–APPL1 interaction measured from this experiment was 0.9 ($\pm$0.7) μM, with k_{on} and k_{off} of 1.3 ($\pm$0.6) $\times 10^3\,M^{-1}\,s^{-1}$, and 1.2 ($\pm$0.4) $\times 10^{-3}\,s^{-1}$, respectively. This k_d value is typical for an interaction between a Rab and its effectors (Eathiraj *et al*, 2005).

A major Rab5-binding site in the PH domain

To identify Rab5-binding site(s) in APPL1, GST–Rab5-Q79L (full length) was used to pull down APPL1 variants having surface point mutations. The WT APPL1 (5–419) fragment was used as the parental construct for the mutagenesis, because this fragment is easily distinguishable from GST–Rab5 by size on SDS–PAGE gels without the need for Western blot analysis. A total of 31 point mutations were made at 27 distinct, solvent-exposed positions (Figure 5; Supplementary Figures 1 and 3), based on the structural information of BAR-PH motif. Most of these point mutations were located in the PH domain or near the BAR–PH interface, which are the surface regions most conserved between APPL1 and APPL2 (Supplementary Figure 5). Substitution mutants were designed to maximize potential mutational effects on Rab5 binding (e.g., by flipping charges or switching between hydrophobic and hydrophilic residues) without disrupting the overall structure. In addition, the flexible L1 loop (residues 289–294) was truncated and replaced with one Gly residue. All of these APPL1 variants, as well as the WT construct, were expressed in *E. coli*, with comparable yields from the soluble fractions (data not shown), in contrast to the mutations at BAR–PH interface mentioned earlier. This suggested that the thirty or so surface mutations had little effect on the stability of BAR-PH dimer. Among them, seven mutants, including V25D, N308D, M310K, A318D, G319R, L321D, and D324A, either abolished or significantly reduced (i.e., retaining <30%) Rab5 binding compared with the WT APPL1 (Figure 5A). In the 3D structure, most of these residues cluster in an elongated surface area formed by β3, L3, and β4 of the PH domain, defining a major Rab5-binding site (Figure 5B; Supplementary Figure 3). In addition, the effect of the V25D mutant suggests that the BAR domain also contributes to Rab binding either directly or indirectly. On the other hand, L1 loop seems not to be required for Rab5 binding; significance of the apparent, positive effect of the truncation mutant (Figure 5A) remains to be studied.

We further extended these binding studies and confirmed the above Rab5-binding site *in vivo* in the cell, by monitoring Rab5-mediated APPL1 recruitment to early endosomes in the cell via confocal microscopy. In this case, the RFP (DsRed-monomer)–Rab5-Q79L fusion protein was expressed in PC12 cells, targeted to the early endosomes, and recruited effectively the coexpressed GFP (green fluorescence protein)–APPL1 to these early endosomes (Figure 5C). Importantly, APPL1 (5–385), that is, the BAR-PH domain, was sufficient to target to Rab5-Q79L containing early endosomes (Figure 5C). In contrast, one of the Rab5-binding defective mutants (A318D) failed to target the early endosomes and exhibited a diffused pattern throughout the cytoplasm in the cell (Figure 5C).

Interaction between small GTPase and BAR domain has been exemplified in a complex crystal structure of Rac and arfaptin2 before (Tarricone *et al*, 2001). Based on the following observations, however, we excluded the possibility of a Rac–arfaptin2-like binding mode for the Rab5–APPL1 interaction. First, the linear dimension of Rab5 is less than 50 Å, which is significantly smaller than the distance (~60 Å) between the putative Rab5-binding site in the PH domain and the central region of the BAR dimmer, where Rac binds with arfaptin2. Second, the isolated APPL1 BAR domain did not bind to Rab5 in our pull-down assay. Third, we mutated APPL1 Asn52, which is at the position equivalent to Rac-binding site in arfaptin2, to either a smaller (Ala) or larger (Arg) side-chain residue, and the mutations showed no effect on the binding to Rab5.

APPL1 as a Rab21 effector

Rab5 subfamily contains several members, including Rab5, Rab21, and Rab22. Among them, Rab5 and Rab22 share a higher overall sequence identity with each other than with Rab21 (Pereira-Leal and Seabra, 2000). This difference was used to explain the ability of Rab5 and Rab22, but not Rab21, to share some common effectors such as EEA1 and rabenosyn5 (Kauppi *et al*, 2002; Eathiraj *et al*, 2005). Therefore, we tested APPL1 binding specificity towards other members in the Rab5 subfamily, using GST–Rab21 (full length) and GST–Rab22 (2–192) to pull down APPL1 (5–419). Interestingly, APPL1 would bind to Rab21 in a GTP-dependent manner (Figure 4), indicating that APPL1 is an effector for both Rab5 and Rab21. On the other hand, we were unable to detect any binding between APPL1 and Rab22 in the pull-down assay (Figure 4). We could not rule out possible *in vivo* interaction between them because our recombinant Rab22 might not have folded correctly in *E. coli* based on the following observations: (1) the expression level of Rab22 was 10- to 20-fold lower than Rab5 and Rab21, and (2) the GTP loading rate of Rab22 was lower too (data not shown). Therefore, we focused our study on Rab5 and Rab21 for their interactions with APPL1. We demonstrated that Rab21 and Rab5 have similar but not identical binding profiles towards APPL1 variants (Figure 5), which may be explained by their sequence divergence. This differential binding to Rab5 and Rab21 by APPL1 may allow *in vivo* analysis of the functional roles of each Rab–APPL1 interaction, for example, by specifically abolishing one interaction while retaining others.

A novel Rab effector binding mode between Rab5 and APPL1

Next we investigated the APPL1-binding regions in Rab5. Since residues responsible for APPL1 binding are likely to be located in the switch I, switch II, and interswitch regions, whose conformations change between different nucleotide binding states, these regions became the main objects of our investigation. In addition to relevant Rab5 mutations that we made in previous studies, several point mutations in the Rab5

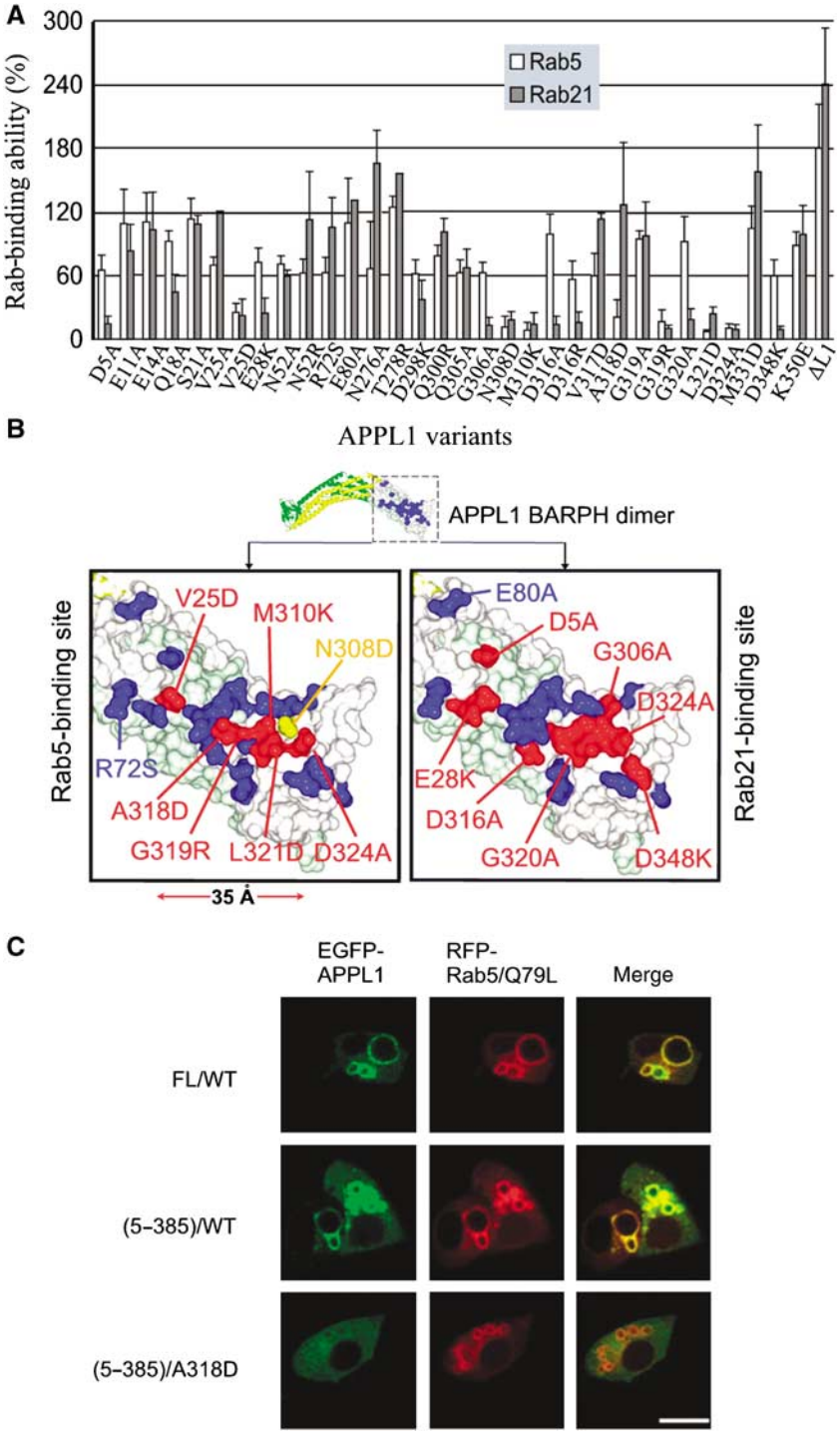

Figure 5 Mutational analyses of APPL1. (**A**) Quantifying the Rab binding ability of APPL1 variants. The Rab5- and Rab21 binding abilities of APPL1 variants relative to that of WT APPL1 (5–419) were estimated based on chemiluminescence-labeled Western blot (see the Materials and methods) and shown as the white and gray bars, respectively. Standard deviations calculated from multiple experiments were represented by the thin lines. (**B**) Mutational effects on binding to Rab5 and Rab21. Distribution of point mutations is shown on the molecular surface of the BAR-PH dimer where the two protomers are colored gray and light green, respectively. APPL1 mutations that affect binding strongly (i.e., <30% binding comparing to WT) are colored red; otherwise, the mutants are colored blue. The position showing reversed binding property is colored yellow. Mutation positions are selectively labeled; note that the PH domain contains residues 276–379. (**C**) Mutational effects on APPL1 targeting to Rab5-positive early endosomes in the cell. RFP–Rab5-Q79L was coexpressed with GFP–APPL1 (full length, FL; BAR-PH domain; or BAR-PH mutant) in PC12 cells as indicated, followed by confocal fluorescence microscopy. Shown are typical confocal microscopic images indicating the RFP–Rab5-Q79L labeled early endosomes (red) and the colocalization of GFP–APPL1 or mutants (green) in the same cells. Scale bar, 16 μm.

switch I region (i.e., residues 40–53) were tested for APPL1 binding. We found that point mutations in the 42–48 region significantly reduced APPL1 binding, while L38R, Q49A, E50A, and I53N showed little or no detectable effect (Figure 6A). Consistent with our previous structural studies on Rab5–rabaptin5 interaction (Zhu *et al*, 2004), all muta-

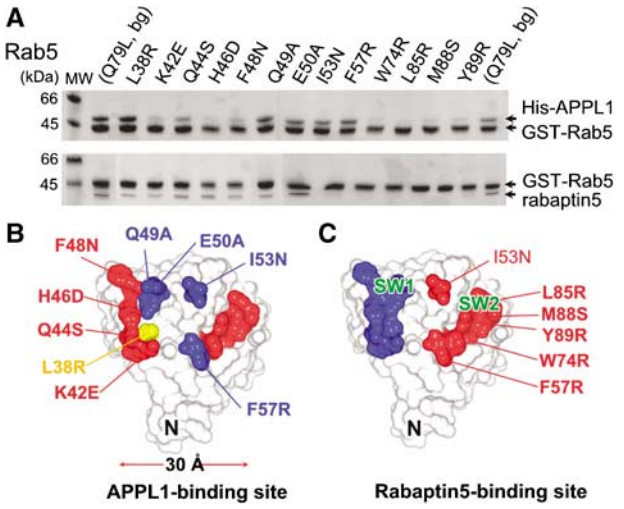

Figure 6 Mutational analyses of Rab5. (**A**) Pull-down assay on Rab5 variants. Point mutations in switch regions were introduced in the full-length Rab5-Q79L background of the GST fusion construct. Each mutant was expressed in *E. coli*, purified, and equal amounts of each Rab5 sample was used to pull down recombinant proteins of His-tagged WT APPL1 (5–419) (top panel) and His-tagged rabaptin5 (551–862) (bottom panel). The results were visualized by Coomassie blue stain. (**B**) Molecular surface model of Rab5 GTPase domain. Its N-terminus, switch I (SW1) and switch II (SW2) regions are labeled. Rab5 mutations that have effects and have no effect on binding are labeled red and blue, respectively. The position showing reversed binding property with the APPL1 N308D mutant is colored yellow.

tions within the 38–50 region did not interfere with Rab5–rabaptin5 binding (Figure 6A). Furthermore, with the knowledge of crystal structures of Rab5–rabaptin5 and Rab22–rabenosyn5 complexes, it is clear that both Rab5 effectors rabaptin5 and rabenosyn5 bind to the so called invariant hydrophobic triad of Rab5 (i.e., Phe57, Trp74, and Tyr89) (Merithew *et al*, 2001). Mutation of any of these residues usually strongly inhibits the Rab-effector binding (Zhu *et al*, 2004; Eathiraj *et al*, 2005). Interestingly, in our mutagenesis analysis, the APPL1-binding was affected by W74R and Y89R, but not by F57R point mutation in Rab5 (Figure 6). Taken together, our results indicate that APPL1 binds to Rab5 regions including the 40–48 loop and switch II, ~30 Å across. In addition, we showed that the two effectors, APPL1 and rapaptin5, could compete for Rab5-binding (data not shown), confirming that the binding sites of APPL1 and rabaptin5 on the Rab5 surface overlap with each other.

To further define the Rab5–APPL1 binding mode, we performed extensive pull-down analyses between variants of Rab5 and APPL1, looking for reversal mutants that could rescue the lost binding ability of others. We identified one such pair; APPL1-N308D abolished the binding to Rab5, while Rab5-L38R had no effect on APPL1 binding. However, Rab5-L38R was found to bind with APPL1-N308D, but not with the other tested APPL1 variants of similar hydrophobic-to-charged mutations, including V25D, A318D, and L321D (Supplementary Figure 6). This result suggests that Rab5-L38R restores binding for APPL1-N308D through complementary, electrostatic, yet specific interactions. It further implies that the position 308 in the β3 strand of APPL1 PH domain is in the vicinity of position 38 in the α1 helix of Rab5 in their complex.

Discussion

BAR-stabilized PH domain is essential for Rab5 binding

Since both APPL1 and APPL2 bind to Rab5, their Rab-binding sites are likely located in a surface region that is conserved between the two APPL proteins. There are no deletion/insertion differences in the BAR-PH region between them (Supplementary Figure 1), and an inspection of the APPL1 BAR-PH dimer surface indicates that the most conserved surface region is located on the PH domain surface and the BAR-PH junction (Supplementary Figure 5). Furthermore, neither PH domain (Miaczynska *et al*, 2004) nor BAR domain alone (data not shown) can directly bind Rab5, suggesting that the dimer interface between PH and BAR domains plays a critical role in Rab5 binding directly or indirectly. This binding mode between Rab5 and APPL1 is apparently distinct from that between Rac and arfaptin, which only requires BAR dimerization (Tarricone *et al*, 2001).

To investigate further the structural basis of APPL1 and Rab5 interaction, we have performed extensive mutagenesis analyses. A BAR dimer breaking mutant (F210D/F211D) and the BAR–PH interface mutant (S16E/P17E) are both insoluble when expressed in *E. coli* (data not shown), supporting the notion that the functional form of APPL1 BAR-PH domain is a dimer. Importantly a series of surface point mutants are soluble, allowing us to analyze the *in vitro* binding properties between these APPL1 mutants and Rab5 (Figure 5). The results indicate that Rab5 specifically binds to the PH domain of APPL1 in the context of BAR-PH dimer, and this binding may marginally extend to the neighboring BAR domain. Our structure-functional analyses are consistent with existing biochemical data. For example, a previously reported triple mutation of APPL1 within the PH domain, K280E/Y283C/G319R, disrupts Rab5 binding (Miaczynska *et al*, 2004). This effect can be fully explained based on the importance of the BAR–PH and PH–Rab5 interfaces.

Combined results from our mutagenesis pull-down experiments (Figures 4–6), crystal structures of the BAR-PH domain of APPL1 (Figure 1), and structures of GTPase domain of human Rab5 in different nucleotide binding modes (Zhu *et al*, 2003, 2004) clearly explain the requirement of GTP-bound Rab5 for APPL1 binding. Based on available information, we have modeled the interaction between the two proteins. With the assumption that both proteins remain rigid bodies, our complex model satisfies constraints imposed by the mutagenesis pull-down results (Figure 7). Over 1200 Å^2 SAS area combined from both the APPL1 dimer and Rab5 would be buried in their interface. In this putative Rab5–APPL1 binding mode, APPL1 interface includes L2, β3, L3, and β4 regions. Note that the L3-β4 region showed weak electron density in the crystal structure, indicating its higher mobility and possible adaptability in forming a complex with Rab5. On the Rab5 side, two regions that harbor binding-defective mutations are involved in the complex formation: the loop 42–48 and switch II (Figure 6). Furthermore, the reversal mutation pair, Rab5-L38R and APPL1-N308D (Supplementary Figure 6) would directly interact with each other inside the interface of our complex model. The bound Rab5 molecules would extend the concave surface of the APPL1 dimer, with both the N- and C-termini of Rab5 exposed to solvent. Considering that there are about 30 residues C-terminal to our Rab5 model, which are necessary for membrane associa-

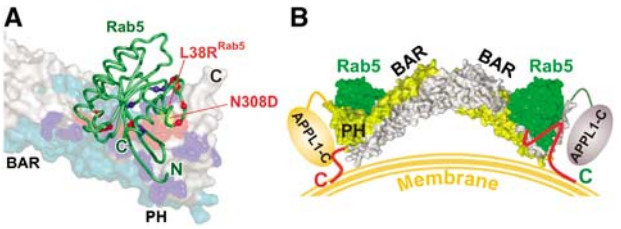

Figure 7 Putative complex model of the APPL1 BAR-PH dimer and Rab5. (**A**) APPL1–Rab5 interaction. The two BAR-PH protomers are shown in molecular surface models and colored gray and cyan, respectively. Positions of APPL1 mutations are colored similarly to Figure 5B. Overlaying APPL1, Rab5 is shown in a green backbone trace and positioned according to the mutagenesis data; the N-and C-termini of its GTPase domain are labeled. Rab5 mutants that affect binding are marked with red spheres, and those having no effect are marked with blue spheres. Positions of the reversal mutation pair are labeled. (**B**) Membrane recruitment of APPL1 mediated by Rab5. The APPL1 BAR-PH protomers are colored gray and yellow, and APPL1 C-terminal peptides are represented by ovals. Rab5 molecules are shown in green molecular surface models, and their membrane anchored C-terminal tails are represented by red curves.

tion but excluded from the crystallography study, our model would allow Rab5 molecules to anchor to the membrane through the added C-terminal tails and to interact with APPL1 at both ends of the BAR-PH dimer (Figure 7). The Rab5 C-terminal tail is likely flexible, supporting that recruitment of APPL1 to the endocytic vesicle may not require its direct contact with the membrane. In the complex, the Rab5 molecule does not block the C-terminus of the PH domain, allowing peptide extension of the APPL1 molecule from the BAR-PH domain.

Rab5–APPL1 interaction represents a novel Rab effector binding mode

In contrast to the α-helix dominant Rab-binding motifs of all other effectors of known 3D structures (Ostermeier and Brunger, 1999; Zhu *et al*, 2004; Eathiraj *et al*, 2005; Wu *et al*, 2005; Wei *et al*, 2006), the Rab5-binding motif of APPL1 is mainly composed of two β-strands, β3 and β4, and their connecting loop L3. Although the exact binding position on the Rab protein and orientation of the effector helices may differ among available complex structures, all these Rab-binding domains interact with the invariant hydrophobic triad. However, we have identified a Rab5 mutation in the hydrophobic triad, F57R, that does not interfere with APPL1 binding, but abolishes the binding to another Rab5 effector, rabaptin5 (Figure 6A; Zhu *et al*, 2004). In contrast, several point mutations in the switch I region of Rab5 affect the binding of APPL1 but not rabaptin5. The 42−48 region in Rab5 has not been previously reported to be involved in effector binding.

GTPase binding has emerged as a major function of PH domains in addition to lipid binding (Lemmon, 2004). For example, PH domains in some guanine nucleotide-exchange factors (GEF) have been shown to bind directly to their cognate small GTPases (Rossman *et al*, 2002, 2003; Lu *et al*, 2004), and our data now show direct interaction between the APPL1 PH domain and Rab5. So far, only two crystal structures of small GTPase−PH domain complexes are available. One is Ran−RanBD1 (PDB file 1RRP). The interactions between the Ran GTPase domain and RanBD1 PH core domain is fairly minor, occurring between the switch I region of the GTPase (equivalent to the 40's in Rab5) and strand β2 of the PH domain. This interaction alone is unlikely to be sufficient to form a stable complex. Indeed, Ran has a long C-terminal peptide beside the GTPase domain, while the PH domain of RanBD1 has an extra N-terminal peptide. These two terminal peptides wrap around the partner proteins forming the major interaction between Ran and RanBD1. Such an interaction seems not to be required for Rab5 and APPL1, because the GTPase domain of Rab5 and BAR-PH domain of APPL1 are sufficient to mediate their interaction. The second published small GTPase−PH complex is that of Ral−Exo84 (PDB file 1ZC3). In this complex, the PH domain of Exo84 uses L1, β5, and L6 to interact with the interswitch and switch II regions of Ral forming an intermolecular β-sheet extension mediated by the PH β5 strand and GTPase β2 strand (Jin *et al*, 2005). Our mutagenesis analysis points to a different surface region (β3, L3, and β4) of the PH domain for Rab5 binding. Therefore, the Rab5−APPL1 interaction represents a new GTPase−PH binding mode.

APPL1 is a representative of BAR-PH containing proteins

Both APPL1 and APPL2 are identified as Rab5 effectors, and their overall aa sequences are highly homologous. In particular, residues on the APPL1 BAR dimer interface, BAR−PH interface, and the presence of the α4 helix seem well conserved in APPL2 (Supplementary Figure 5). Therefore, APPL2 BAR-PH domain most likely forms a homodimer very similar to that of APPL1. Furthermore, these conserved structural features may also extend to other BAR-PH containing proteins (Supplementary Figure 1; Habermann, 2004). For instance, no helix breaking aa sequence appears in the middle of their predicted α4 regions. Based on the APPL1 BAR-PH crystal structure, we find that, in general, the PH domain is more conserved than the BAR domain, and most of the highly conserved positions are located closer to the BAR−PH interface rather than the central region of the symmetric dimer. For example, the two major contact regions between PH and BAR domains (i.e., D^{15}SPxxR^{20} and D^{334}xxDRRYCF^{342}) are conserved at the aa sequence level among BAR-PH containing proteins. In addition, correlated mutations are present between these proteins at the BAR−PH interface. Thus, we propose that all BAR-PH containing proteins share similar 3D structures in the corresponding regions and that the BAR-PH motif may function as a general structural unit to interact with membrane-bound proteins and other molecular moieties.

In some BAR containing proteins, it is proposed that there exists an amphipathic helix N-terminal to the α1 helix of BAR domain, and they are called an N-BAR motif (Peter *et al*, 2004; Gallop *et al*, 2006). It is suggested that this extra N-terminal region facilitates membrane binding (or bending). A similar N-BAR structure was predicted for APPL1 and APPL2 (Habermann, 2004), but our current APPL1 crystal structure does not show such a structural motif. Instead, the N-terminal region assumes an extended conformation and packs in the groove formed between helices α1 and α3 on the convex side of the crescent-shaped dimer (Figure 3C). Since the N-terminal regions of the other BAR-PH containing proteins (Supplementary Figure 1) share similar sequences, we suggest that none of these proteins contains an N-BAR motif in their 3D structure.

Lacking both the amphipathic helix N-terminal to the BAR domain and the lipid-binding motif in the PH domain (Supplementary Figure 1) may explain the Rab5-dependent membrane association of APPL1. In contrast, the PH domains of centaurin-β1/2 contain the key, basic residues for phosphoinositide binding (Dinitto and Lambright, 2006; Supplementary Figure 1). If their PH domains are oriented similarly to that in the APPL1 dimer, the canonical (i.e., L1–L3–L6), ligand-binding triangle in their PH domains likely contributes to direct membrane association of these proteins.

Functional implications of the BAR-PH structure

While it is suggested that Rab5−APPL1 interaction mediates a signal transduction pathway between the plasma membrane and the nucleus, the mechanism by which Rab5 binding stimulates APPL1 translocation to the nucleus remains elusive. The current BAR-PH structure may help to clarify the mechanism. Interestingly, the sequence of 'PKKKENE' was identified in the BAR domain of APPL2 as a potential nuclear localization signal (Miaczynska *et al*, 2004). The corresponding region in APPL1 is the solvent exposed loop connecting α2 and α3 at the tip of the dimer (Figure 1B) and has a fairly conserved sequence (Supplementary Figure 1). In addition, our preliminary data suggest that there is no detectable binding between the BAR-PH domain and the C-terminal region of APPL1 (data not shown), which makes it unlikely that Rab5 may regulate APPL1 through interference with the intramolecular interaction of the latter. It seems more probable that the Rab5−APPL1 complex recruits downstream effectors to propagate the signal transduction process.

Unlike other Rab effectors, APPL1/2 proteins function in the signaling pathway from the so-called signaling endosome to nucleus. Our data show that APPL1 interacts with the Rab5 protein using a novel binding mode; it remains to be proven whether such a binding mode is essential for APPL1 function. Whereas it has been shown that APPL1 does not bind other Rab proteins miscellaneously (Miaczynska *et al*, 2004), we demonstrate that APPL1 is also an effector of Rab21, indicating that APPL1 adopts a binding mode shared by both Rab5 and Rab21. It raises the possibility that, besides Rab5, other members of this Rab subfamily may also be involved in the APPL1 signaling pathway.

Materials and methods

Protein expression and purification

Constructs of human APPL1 (GenBank ID: NP_036228) (5−265) (i.e., the BAR domain) and APPL1 (5−385) (i.e., the BAR-PH domain) were inserted into the vectors pET28a and pET15b (Novagen), respectively, between *Nde*I and *Bam*HI restriction sites. The N-terminal few residues in the native sequence are hydrophobic and were deleted in an attempt to improve the solubility. Point mutations were introduced into the pET15b-APPL1 (5−419) parental construct using QuickChange™ site-directed mutagenesis kit (Stratagene).

His-tagged proteins of APPL1 (5−265) and APPL1 (5−385) were expressed as soluble recombinant proteins in BL21 Star™ (DE3) strain of *E. coli* (Invitrogen), and cells were harvested after induction with 0.1 mM isopropyl-β-D-thiogalactopyranoside (IPTG) for 8 h at 25°C. The cells were lysed with lysozyme, and the lysate supernatant was purified with His-Select™ affinity beads (Sigma). In both cases, the His tag was removed with thrombin. After further purification with Resource-Q™ anion-exchange chromatography (GE Healthcare), both protein samples were concentrated to ~30 mg ml^{-1} in (20 mM Tris–HCl (pH 8.0) and 0.1% (v/v) β-mercaptoethanol (βME)) and stored at −85°C until needed. APPL1 (5−419) mutants were expressed similarly. Se-Met-substituted proteins were expressed in *E. coli* B834 (DE3) pLysS cells (Novagen) in minimal media supplemented with 40 mg l^{-1} Se-Met (Sigma) and purified using the same procedure as the native protein.

Recombinant proteins of human Rab5a variants (GenBank ID: NM_004162), human Rab21 (BC021901), and human Rab22a (NM_020673) fused with an N-terminal GST were expressed in BL21 *E. coli* and purified with GST-affinity chromatography. The sample was concentrated to ~20 mg ml^{-1} and stored in 1× phosphate-buffered saline (PBS) with 0.1% (v/v) βME at −80°C. Recombinant protein of human rabaptin5 (551–862) (GenBank ID: CAA62580) was expressed and purified as described previously (Zhai *et al*, 2003); two additional point mutations, C719S and C734S, were introduced to reduce aggregation.

Protein crystallization and data collection

Crystals of APPL1 (5–265) were grown at 20°C with the hanging drop vapor diffusion method. The Se-Met incorporated protein sample diluted to 10–20 mg ml^{-1} was mixed 1:1 (v/v) with the reservoir solution of 0.1 M magnesium formate and 0.1% (v/v) βME. Crystals were transferred to a cryo-protectant solution of (88% saturated Li_2SO_4, 14 mM magnesium formate, 20 mM Tris–HCl (pH 8.0), and 0.1% (v/v) βME) by gradually changing the drop solution in 20 min, followed by cooling in liquid nitrogen. A data set was collected at selenium edge at sector 22 BM of the Argonne APS facility.

Crystals of APPL1 (5–385) were also grown in hanging drops at 20°C. The reservoir contained 6% (w/v) polyethylene glycol 6000 (PEG6K), 0.6 M NaCl, and 0.1% (v/v) βME. The crystals were quickly soaked in a solution of (7.5% (w/v) PEG6K, 0.25 M NaCl, and 10% (v/v) glycerol) and flash-cooled under liquid nitrogen. Both native and SAD data sets were collected at the APS facility. Analyzing the crystal content by SDS–PAGE confirmed the integrity of the protein sample. All data were processed with the program suite HKL2000.

Pull-down assay for analyzing protein–protein interactions

In the Rab5−APPL1 pull-down experiment, 30 μg GST−Rab fusion protein (52 kDa) was incubated with 60 μl of 30% slurry of GSH–Sepharose 4B (GE Healthcare) at 22°C for 30 min. Nucleotide loading reaction was performed on the GSH beads in an exchange buffer of (1× PBS, 2 mM DTT, 1 mM $MgCl_2$, 4 mM EDTA, and 400 μM GppNHp or GDP) at 22°C for 30 min. Increasing the magnesium ion concentration to 20 mM terminated the loading reaction. Soluble fractions of cell lysate containing all His-tagged APPL1 (5–419) variants were analyzed by SDS–PAGE to confirm their comparable expression level and solubility. The GSH resin carrying nucleotide-loaded GST−Rab fusion protein was incubated with ~50 μl cell lysate (~200 μg APPL1 variant, 50 kDa) at 22°C for 30 min, then washed three times with 200 μl of (1× PBS, 2 mM DTT, and 4 mM $MgCl_2$) and resuspended in 20 μl of 2× reducing SDS sample buffer. The sample was subjected to SDS–PAGE analysis, visualized with Coomassie blue stain. The same samples were analyzed with chemiluminescence Western blot (GE Healthcare) and His-tag antibody then detected on films which were semi-quantified using the computer software ImageJ (http://rsb.info.nih.gov/ij/) including its default calibration. The relative band intensity of each mutant versus WT from multiple experiments is shown in Figure 5.

Coordinate deposit

Coordinates and the structural factors of the APPL1 crystal structures have been deposited to PDB under codes 2Q12 (BAR domain structure) and 2Q13 (BAR-PH domain structure).

Supplementary data

Supplementary data are available at *The EMBO Journal* Online (http://www.embojournal.org).

Acknowledgements

We thank Drs YQ Chen and H Chial of Wake Forest University for the gift of APPL1 cDNA; X Yu and P Wei for assistance in the AUC experiments; W Li and Y Chen for assistance in the SPR experiments; Z Zhou and M Zhang for technical assistance; Dr T Mather for helpful discussion. This project was supported in part by the Oklahoma Center for the Advancement of Science and Technology (US, grant HR03-147 to XCZ), NIH (US, grant GM074692 to GL), and CAS (China, grant 2006CB911002 to XL).

References

Carlton J, Bujny M, Peter BJ, Oorschot VM, Rutherford A, Mellor H, Klumperman J, McMahon HT, Cullen PJ (2004) Sorting nexin-1 mediates tubular endosome-to-TGN transport through coincidence sensing of high- curvature membranes and 3-phosphoinositides. *Curr Biol* **14:** 1791–1800

Dinitto JP, Lambright DG (2006) Membrane and juxtamembrane targeting by PH and PTB domains. *Biochim Biophys Acta* **1761:** 850–867

Eathiraj S, Pan X, Ritacco C, Lambright DG (2005) Structural basis of family-wide Rab GTPase recognition by rabenosyn-5. *Nature* **436:** 415–419

Farsad K, Ringstad N, Takei K, Floyd SR, Rose K, De Camilli P (2001) Generation of high curvature membranes mediated by direct endophilin bilayer interactions. *J Cell Biol* **155:** 193–200

Gallop JL, Jao CC, Kent HM, Butler PJ, Evans PR, Langen R, McMahon HT (2006) Mechanism of endophilin N-BAR domain-mediated membrane curvature. *EMBO J* **25:** 2898–2910

Habermann B (2004) The BAR-domain family of proteins: a case of bending and binding? *EMBO Rep* **5:** 250–255

Jin R, Junutula JR, Matern HT, Ervin KE, Scheller RH, Brunger AT (2005) Exo84 and Sec5 are competitive regulatory Sec6/8 effectors to the RalA GTPase. *EMBO J* **24:** 2064–2074

Kauppi M, Simonsen A, Bremnes B, Vieira A, Callaghan J, Stenmark H, Olkkonen VM (2002) The small GTPase Rab22 interacts with EEA1 and controls endosomal membrane trafficking. *J Cell Sci* **115:** 899–911

Lemmon MA (2004) Pleckstrin homology domains: not just for phosphoinositides. *Biochem Soc Trans* **32:** 707–711

Li G (1996) Rab5 GTPase and endocytosis. *Biocell* **20:** 325–330

Lin DC, Quevedo C, Brewer NE, Bell A, Testa JR, Grimes ML, Miller FD, Kaplan DR (2006) APPL1 associates with TrkA and GIPC1 and is required for nerve growth factor-mediated signal transduction. *Mol Cell Biol* **26:** 8928–8941

Liu J, Yao F, Wu R, Morgan M, Thorburn A, Finley Jr RL, Chen YQ (2002) Mediation of the DCC apoptotic signal by DIP13 alpha. *J Biol Chem* **277:** 26281–26285

Lu M, Kinchen JM, Rossman KL, Grimsley C, deBakker C, Brugnera E, Tosello-Trampont AC, Haney LB, Klingele D, Sondek J, Hengartner MO, Ravichandran KS (2004) PH domain of ELMO functions in trans to regulate Rac activation via Dock180. *Nat Struct Mol Biol* **11:** 756–762

Mao X, Kikani CK, Riojas RA, Langlais P, Wang L, Ramos FJ, Fang Q, Christ-Roberts CY, Hong JY, Kim RY, Liu F, Dong LQ (2006) APPL1 binds to adiponectin receptors and mediates adiponectin signalling and function. *Nat Cell Biol* **8:** 516–523

Merithew E, Hatherly S, Dumas JJ, Lawe DC, Heller-Harrison R, Lambright DG (2001) Structural plasticity of an invariant hydrophobic triad in the switch regions of Rab GTPases is a determinant of effector recognition. *J Biol Chem* **276:** 13982–13988

Miaczynska M, Christoforidis S, Giner A, Shevchenko A, Uttenweiler-Joseph S, Habermann B, Wilm M, Parton RG, Zerial M (2004) APPL proteins link Rab5 to nuclear signal transduction via an endosomal compartment. *Cell* **116:** 445–456

Mitsuuchi Y, Johnson SW, Sonoda G, Tanno S, Golemis EA, Testa JR (1999) Identification of a chromosome 3p14.3–21.1 gene, APPL, encoding an adaptor molecule that interacts with the oncoprotein-serine/threonine kinase AKT2. *Oncogene* **18:** 4891–4898

Nechamen CA, Thomas RM, Dias JA (2007) APPL1, APPL2, Akt2 and FOXO1a interact with FSHR in a potential signaling complex. *Mol Cell Endocrinol* **260–262:** 93–99

Ostermeier C, Brunger AT (1999) Structural basis of Rab effector specificity: crystal structure of the small G protein Rab3A complexed with the effector domain of rabphilin-3A. *Cell* **96:** 363–374

Pereira-Leal JB, Seabra MC (2000) The mammalian Rab family of small GTPases: definition of family and subfamily sequence motifs suggests a mechanism for functional specificity in the Ras superfamily. *J Mol Biol* **301:** 1077–1087

Peter BJ, Kent HM, Mills IG, Vallis Y, Butler PJ, Evans PR, McMahon HT (2004) BAR domains as sensors of membrane curvature: the amphiphysin BAR structure. *Science* **303:** 495–499

Rebecchi MJ, Scarlata S (1998) Pleckstrin homology domains: a common fold with diverse functions. *Annu Rev Biophys Biomol Struct* **27:** 503–528

Rossman KL, Cheng L, Mahon GM, Rojas RJ, Snyder JT, Whitehead IP, Sondek J (2003) Multifunctional roles for the PH domain of Dbs in regulating Rho GTPase activation. *J Biol Chem* **278:** 18393–18400

Rossman KL, Worthylake DK, Snyder JT, Siderovski DP, Campbell SL, Sondek J (2002) A crystallographic view of interactions between Dbs and Cdc42: PH domain-assisted guanine nucleotide exchange. *EMBO J* **21:** 1315–1326

Sakamuro D, Elliott KJ, Wechsler-Reya R, Prendergast GC (1996) BIN1 is a novel MYC-interacting protein with features of a tumour suppressor. *Nat Genet* **14:** 69–77

Tarricone C, Xiao B, Justin N, Walker PA, Rittinger K, Gamblin SJ, Smerdon SJ (2001) The structural basis of arfaptin-mediated cross-talk between Rac and Arf signalling pathways. *Nature* **411:** 215–219

Varsano T, Dong MQ, Niesman I, Gacula H, Lou X, Ma T, Testa JR, Yates III JR, Farquhar MG (2006) GIPC is recruited by APPL to peripheral TrkA endosomes and regulates TrkA trafficking and signaling. *Mol Cell Biol* **26:** 8942–8952

Wei J, Fain S, Harrison C, Feig LA, Baleja JD (2006) Molecular dissection of Rab11 binding from coiled-coil formation in the Rab11-FIP2 C-terminal domain. *Biochemistry* **45:** 6826–6834

Wu M, Wang T, Loh E, Hong W, Song H (2005) Structural basis for recruitment of RILP by small GTPase Rab7. *EMBO J* **24:** 1491–1501

Zhai P, He X, Liu J, Wakeham N, Zhu G, Li G, Tang J, Zhang XC (2003) The interaction of the human GGA1 GAT domain with Rabaptin-5 is mediated by residues on its three-helix bundle. *Biochemistry* **42:** 13901–13908

Zhu G, Liu J, Terzyan S, Zhai P, Li G, Zhang XC (2003) High resolution crystal structures of human Rab5a and five mutants with substitutions in the catalytically important phosphate-binding loop. *J Biol Chem* **278:** 2452–2460

Zhu G, Zhai P, Liu J, Terzyan S, Li G, Zhang XC (2004) Structural basis of Rab5–Rabaptin5 interaction in endocytosis. *Nat Struct Mol Biol* **11:** 975–983